



Pollutant Dispersion Around a Single Tall Building

Tomos Rich¹ · Christina Vanderwel¹

Received: 14 March 2024 / Accepted: 29 June 2024
© The Author(s) 2024

Abstract

An experiment was carried out using a scale model of a tall building, with the goal of investigating the role of individual buildings in the dispersion of air pollution. Pollutant dispersion around an isolated building with a height-to-length aspect ratio of 1.4 is investigated using simultaneous particle image velocimetry and planar laser induced fluorescence. Dye is released from a ground-level point source five building heights upstream of the tall building. It was found that in this case the scalar plume was dispersed laterally strongly by the building, but only slightly vertically. It is hypothesized that this is due to 94% of the plume impinging below the stagnation point on the front of the building and being drawn into the horseshoe vortex. We expect this fraction would be lower in a case in which the building is in an array of smaller buildings, and that this would lead to more vertical dispersion.

Keywords Atmospheric boundary layer · Air pollution dispersion · Particle image velocimetry · Scale model experiment · Urban aerodynamics

1 Introduction

Urban air pollution is becoming an important global problem as the proportion of the world's population living in urban environments increases. Currently this proportion is at 55% and this figure is predicted to rise to 68% by 2050 (United Nations Department of Economic and Social Affairs 2018). There is now a better understanding of how the negative health effects of living with air pollution can be severe (Dziubanek et al. 2017). The World Health Organisation estimates that in 2019, 6.7 million premature deaths were caused by air pollution and of these 4.2 million were caused by outdoor air pollution. As a growing proportion of the world's population resides in cities and is exposed to this pollution, the importance of predicting it correctly has been emphasized.

Understanding urban airflow and how air pollution is transported is necessary for both weather forecasting and air quality forecasting. In the UK, two of the main providers of these data types respectively are the Met Office and the Department of Environment, Food, and

✉ Christina Vanderwel
C.M.Vanderwel@soton.ac.uk

Tomos Rich
tjr1u19@soton.ac.uk

¹ University of Southampton, Southampton, UK

Rural Affairs. The Met Office uses High Performance Computer (HPC) powered computational models so that they are able to output daily forecasts of weather and air quality (Met Office 2022; Bermous and Steinle 2015). The Department of Environment, Food, and Rural Affairs uses a variety of models to predict pollution, some running on HPC and some more simple ones that can be run on personal computers (Williams and Barrowcliffe 2011). It has also recently become necessary for new building developments within London to conduct studies into the influence they will have on the local urban micro-climate (City of London 2022).

The scalar transport equation must be solved in order to predict air pollution dispersion and this equation is given by:

$$\frac{\partial C}{\partial t} + U_j \frac{\partial C}{\partial x_j} = \frac{\partial}{\partial x_j} \left(\gamma \frac{\partial C}{\partial x_j} - \overline{c'u'_j} \right). \quad (1)$$

Here, the C term refers to the time-averaged concentration of a flow, and the U_j term refers to the time-averaged flow velocity in the j direction. In a simulation this requires modelling of the turbulent flux term which is given by $-\overline{c'u'_j}$ in Eq. 1, due to this term being comprised of fluctuating components (Pope 2001; Arya et al. 1999). This is true for either Reynolds averaged Navier Stokes or large eddy simulations; however, in direct numerical simulations or experimental studies, this term is accurately simulated. In contrast, the advective scalar dispersion ($U_j \frac{\partial C}{\partial x_j}$) are fully resolved in all of these simulation types.

Experiments show that within an urban boundary layer this turbulent flux is often at least one order of magnitude lower than the advective flux (Talluru et al. 2018). However the direction of this flux does not necessarily agree with that of the advective flux. A previous study by our team at the University of Southampton (Lim et al. 2022) found that for a particular scalar release the turbulent flux was significant to vertical transport, but only over the rooftop shear layer of one building in the path of the plume. The gap in understanding in this previous study is how inhomogenous low level buildings contributed to this particular case.

The objective of this work is to use experiments to measure a scalar release around an isolated building in a more comprehensive manner than just center-line measurements. By comparing our findings with those of Lim et al. (2022), we aim to reveal the role of upstream buildings or lack thereof. We also quantitatively present both the turbulent and scalar fluxes in multiple cross-sections of the flow.

2 Literature Review

Understanding flow features around buildings can be approached through the study of simplified structures, with the most simple of all being the flow around a cube. The characteristics of a fluid flow over a single cube have been previously studied (Martinuzzi and Tropea 1993; Xie et al. 2008; Hearst et al. 2016). In the diagram shown in Fig. 1a, a horse-shoe vortex forms below the stagnation point ahead of the cube. The large attached vortex in the wake of the cube is shown in Fig. 1b. These two vortices are particularly significant for bluff bodies with a relatively low height-to-length aspect ratio like cubes. The small vortices visible in Fig. 1a on the top and side of the cube are also common to most bluff bodies and indicate flow separation. Castro and Robins (1977) observed that the reattachment of flow behind these vortices depends on the turbulence intensity of the flow and the ratio of boundary layer depth to cube height. Castro and Robins (1977) also found that in the wake

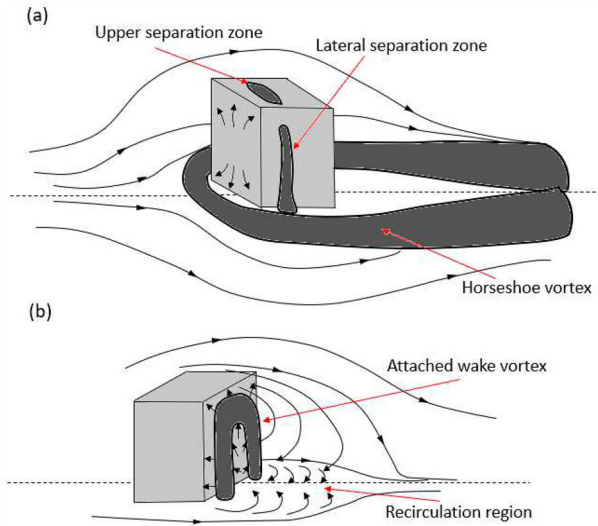


Fig. 1 **a** The flow structures around the front, top, and side faces of a bluff body attached to a wall. **b** The flow structures in the wake of the same bluff body. Both **(a)** and **(b)** are inspired by the work of Martinuzzi and Tropea (1993)

of a wall mounted cube, the mean stream-wise velocity profile past the cube varied by only a few percent from the freestream at a downstream distance of $4.5H$, and variation was below experimental uncertainty levels of their hot-wire measurements by $8.5H$. This is not to say that the flow was back to entirely free-stream conditions, turbulent statistics take longer to reform to background levels than mean flow does. In this case by Castro and Robins, reversed flow was observed to extend just slightly more than one cube height downstream.

The Commonwealth Advisory Aeronautical Research Council (CAARC) tall building model is another standardised bluff body used for investigations with a higher aspect ratio than a cube (Elshaer et al. 2016). The CAARC building's height-to-length aspect ratio is equal to 6 when aligned with its wider face to the flow. The CAARC building creates the same pattern of vortices and detached flow as a cube, however, in this higher aspect ratio case certain vortices are expanded or contracted. Braun and Awruch (2009) shows the lateral vortices shedding from the cube sides are elongated vertically in proportion to the building height. It is also shown that the vertical recirculation region detaching from the top-back edge only propagates halfway down the height of the building in this case, and extends less than one building height downstream.

Both high and low aspect ratio bluff bodies share the flow structures presented in Fig. 1a, b. In the case of high aspect ratio buildings like the CAARC building, the lateral and cross stream sections of the rear detached vortices stretch the full height of the building (Zhao et al. 2022). The horseshoe vortex and the vertical recirculation in the rear are also proportionally weaker (Hu and Morgans 2022). In contrast to this for low aspect ratio bluff bodies such as cubes, all vortices are present but the horseshoe and vertical recirculation sections are more relevant to the flow (Castro and Robins 1977). While the influence of aspect ratio on the flow structure around the building is fairly well understood, its impact on scalar dispersion has been less thoroughly studied.

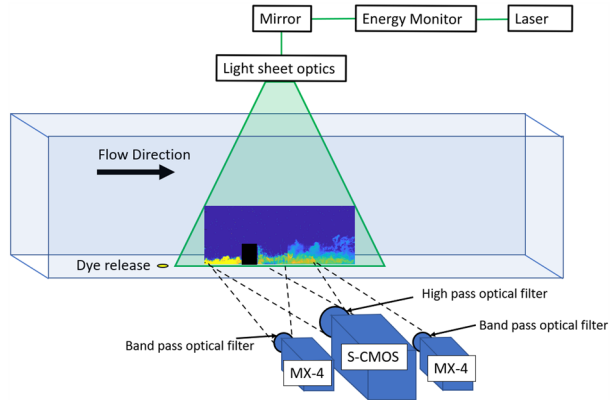
Several studies also consider a single tall building surrounded by low lying urban environment. It has been shown that the presence of one building like this can be significant to both the velocity and scalar concentration fields. Fuka et al. (2018) measured the effect of adding a single tall building with a height-to-length aspect ratio of 3 to a uniform array of low buildings, both experimentally and computationally. They took combined velocity-concentration measurements, allowing both the advective and turbulent scalar fluxes to be examined. They found that the tall building created an area in its vicinity with lower vertical transport, both advective and turbulent, but with higher lateral transport. In contrast, the low buildings by themselves created mostly negative vertical advective fluxes, at low heights, but large, positive vertical turbulent fluxes, that resulted in overall upwards vertical species transport. The flow field shows that this is in part because species in front of the tall building, at a low height, gets caught in the strong down-wash and horseshoe vortex pattern. Fuka et al also suggested a high sensitivity to the scalar source location, which is in agreement with the findings of Fackrell and Robins (1982).

The changes in dispersion measured by Fuka et al. (2018) when changing the scalar source position can be interpreted through the flow structures into which the scalar is being released. Fuka et al. (2018) investigated a case with the species release in the street canyon slightly ahead of the tall building and to the side, and showed a similar flow pattern to the uniform array case, aside from an asymmetric deflection away from the wake of the tall building. This appears to reveal the species being trapped in the horseshoe vortex emanating from the tall building. In a different case in which scalar was released into the wake of the tall building directly, the species became trapped in the near wake of the building within the recirculation region. This release point showed the least horizontal transport, and by far the most vertical transport. It appears that species entering this taller recirculation zone is strongly vertically transported by the rooftop shear layer; however, most species impacting the front of the building is transported horizontally away from this zone, so it mostly stays relatively clear of the species. Heist et al. (2009) shows that in the case that the scalar is released at ground level directly into the recirculation bubble, vertical transport of the scalar is significantly higher than elsewhere in the uniform array, agreeing with the latter study by Fuka et al.

In a more recent study, Lim et al. (2022) studied dispersion around a tall building with a height-to-length aspect ratio of 1.4 situated in a realistic neighbourhood of low-rise buildings using experiments and computational simulations. They found that a significant proportion of the scalar was transported above the building and spread vertically by the detached shear layer at the top of the rear vortex. They also measured the relative significance of the advective and turbulent fluxes and identified a strong correlation between the turbulent stresses and the vertical scalar transport in the upper region of the wake. This contrasts the findings of Fuka et al. (2018) and could be a result of the different surrounding building geometries and building aspect ratio in both cases.

Airflow in urban environments often has a Reynolds number in the order of magnitude of hundreds of thousands or millions. Experimental investigations into these subjects are limited by facility size to Reynolds numbers of the order of 10,000. Fortunately it has been proven that bluff bodies become Reynolds number independent at a Reynolds number of roughly 10,000–20,000 (Castro and Robins 1977; Plate 1999). This is due to the sharp edges of bluff bodies creating fixed separation points, which are relatively insensitive to viscous effects. Therefore in an urban case in which buildings are modelled as bluff bodies, the flow structures present around these bluff bodies are insensitive to flow velocity above this region of Reynolds numbers.

Fig. 2 A diagram of the streamwise measurement setup used for planar PIV and PLIF. This three camera setup allows measurement of an area $4H$ tall by $7H$ wide (120 mm by 210 mm)



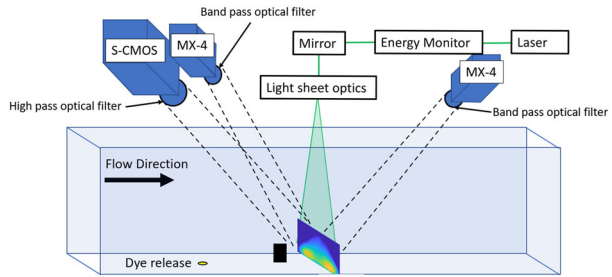
The objective of this work is to investigate scalar dispersion around an isolated tall building using novel experimental techniques that provide full maps of both the turbulent and advective fluxes, and to use this data to draw conclusions about the interaction between the scalar and the flow structures. The value of this lies in the variation shown by previous studies in how a scalar is transported through the regions in which these flow structures are expected. By calculating both fluxes, a clearer picture of the components of scalar transport can be created. In addition, the building aspect ratio of 1.4 was chosen so that comparison could be made with the study by Lim et al. (2022), so that the effect of a surrounding low lying urban environment to this tall building could be investigated through its absence.

3 Methodology

This investigation was carried out in the recirculating water tunnel at the University of Southampton. This facility has a total test section length of 8 ms , width of 1.2 ms , and maximum depth of 1 m . For all measurements the water depth was constant at 0.5 ms and the velocity was 0.55 m/s . The building itself was modelled on a particularly tall building in the city section used by Lim et al. (2022), which was based on a neighborhood in Beijing. Lim et al studied this at a scale of 1:2400. It was approximated as a single square cylinder with a height of $H = 30\text{ mm}$ and length of $L = 21.4\text{ mm}$, resulting in an aspect ratio of $H/L = 1.4$. This places it physically in between the CAARC building (Braun and Awruch 2009; Elshaer et al. 2016) with an aspect ratio of 6 and a cube with an aspect ratio of 1. The experimental Reynolds number based on the building height and the constant free-stream speed of 0.55 m/s was 16,424. This is high enough that flow around this building can be assumed to be Reynolds independent (Plate 1999; Lim et al. 2007).

Dye was released upstream of the building a distance of $x_F = 5H = 150\text{ mm}$ from the front of the building, which is equal to a distance of $x_B = 5.71H = 171.4\text{ mm}$ from the back of the building. This was sufficient for the plume to have dispersed a moderate amount in the boundary layer prior to impacting the building and has the additional effect of moving the interaction between the plume and the building outside the near-source region (Lim and Vanderwel 2023). Dye was used as it is a passive scalar in water, and therefore it was used as a proxy for air pollution. The dye release was at a rate of $10\text{ cm}^3/\text{min}$ from a point source and at a 45° angle to the flow. This dye injection was found to not have a measurable effect

Fig. 3 A diagram of the cross-stream measurement setup used for stereo PIV and PLIF. This setup allows measurement of an area 7 H tall by 5 H wide (210 mm by 150 mm)



on the local flow velocity. An isokinetic ground level point source was used to reduce any influence that source characteristics might have on the experiment, as previous literature has shown that experiments on scalar plumes are highly sensitive to source conditions (Fuka et al. 2018).

Measurements were taken using coupled 2D particle image velocimetry (PIV)—planar laser induced fluorescence (PLIF) along the centre plane of the flow in the streamwise direction. The field of view extended four building heights upstream of the building and 14 building heights downstream. This required recording using a pair of side by side Lavision MX-4 cameras for PIV, along with a Lavision S-CMOS camera for PLIF. The Lavision S-CMOS was chosen for PLIF due to its 16 bit pixel depth. A calibration plate was used to align each of the cameras and we estimate any errors due to misalignment of the coordinate systems would be less than 0.1 mm. This three-camera setup was used in three different locations to create three datasets captured at different times. A diagram of the three-camera experimental setup is shown in Fig. 2.

The dye used in this study was Rhodamine 6 G, which has a Schmidt number $Sc = \nu/D = 2500 \pm 300$ where ν is the kinematic viscosity and D is the mass diffusivity (Vanderwel and Tavoularis 2014). This means that momentum diffusion is much faster than scalar diffusion. Rhodamine 6 G is fluorescent and absorbs light at a wavelength of 525 nm and reemits at 554 nm. A Litron ND:YAG Nano pulsed laser was used as the illumination for both PIV and PLIF, which emitted at a wavelength of 532 nm and an average pulse energy of 400 mJ. Equipping the S-CMOS used for PLIF with a long-pass filter at 540 nm filters out all laser light and allows through only reemitted fluorescent light. The MX-4 cameras were equipped with band pass filters that allowed the 532 nm laser-light through, which allowed them to measure particle displacement within the fluorescing dye plume.

Coupled Stereo PIV–PLIF measurements were also taken in cross-stream slices downstream of the building in six planes, each separated by two building heights. The first of these was 2 H downstream of the back of the tall building and 7.71 H downstream of the dye source. The experimental setup for this is shown in Fig. 3. For all measurements, data was collected at 10 Hz for 200 s, giving 2000 total PIV image pairs and PLIF images. Convention in this paper is to take the origin as the dye release unless stated otherwise, and to take downstream direction as x , cross-stream as y , and vertical as z .

A bootstrap method was used on the first and second order statistics of both the PIV and PLIF datasets using five points within the plume. For PIV it was found that the standard error in the mean streamwise velocity was 1%, and the standard error in the $\overline{u'u'}$ variance of the fluctuating velocity was 2%. For PLIF, it was found that the standard error in mean concentration was 1%, and the standard error in the variance ($\overline{c'c'}$) was 5%. This provides confidence that 2000 samples was sufficient for converged statistics.

Fig. 4 A photo taken inside the University of Southampton's recirculating water tunnel while fully drained. This photo is taken from the test section looking upstream, it shows the upstream roughness and spires used to generate an incoming atmospheric boundary layer



In turbulent flows it becomes necessary to take measurements with a range of dye concentrations in order to maintain a good signal to noise ratio. The measured local concentrations are normalised by the source concentration. This is valid if the locally measured concentration is within the linear response regime (ie. < 0.6 mg/L). The source concentration was chosen to obtain the maximum concentration in the field of view, which did not overexpose the camera. In some cases where the species concentration varies by more than an order of magnitude within one field of view, such as near the source, multiple measurements with varying source concentrations were stitched together. The dye source concentrations used in this study varied from 1 to 60 mg/L.

Urban environments currently always exist within an atmospheric boundary layer. Therefore in order to experimentally model an urban environment with any accuracy, an atmospheric boundary layer must also be modelled. This can be done through the use of uniform roughness elements and larger spire structures (Tomas et al. 2017). In this experiment, the atmospheric boundary layer was modelled using the flow conditioning shown in Fig. 4. This roughness is comprised of spires followed by descending sizes of roughness elements, from 2 to 1 cm² then to 0.5 cm².

The boundary layer formed for this experiment had a depth at the test section of 103 mm and varied less than 2% within the field of view. Details of the freestream flow characteristics are shown in Fig. 5. With the building height of 30 mm this boundary layer depth is sufficient to keep the building height within the log-law region of the boundary layer. The log law region is visible in Fig. 5b which presents the velocity profile scaled by wall units. This is significant as this is true for a realistic city case. Using the peak of the Reynolds shear stress to calculate the friction velocity gives a value of (0.019 ± 0.001) ms⁻¹, and a friction Reynolds number $Re_{\tau} = 1500$.

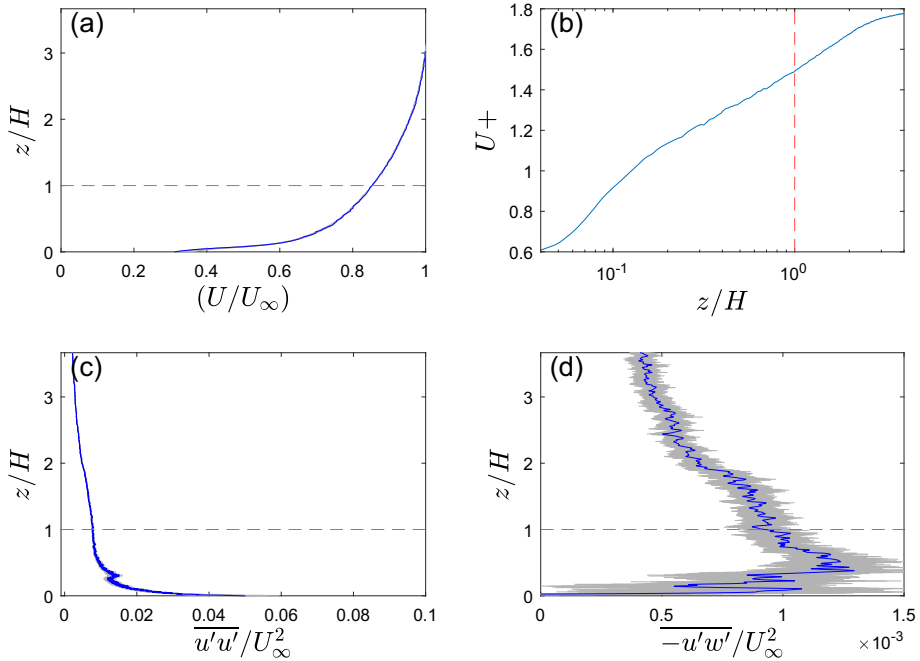


Fig. 5 **a** The incoming streamwise flow velocity U/U_∞ . **b** The incoming streamwise flow velocity normalised by the friction velocity (U^+), plot on a semilog scale so that the log law region of the boundary layer can be observed. **c** The profile of the variance of the streamwise velocity $\overline{u'u'}/U_\infty^2$ of the incoming flow. **d** The profile of the Reynolds stress $-\overline{u'w'}/U_\infty^2$ of the incoming flow. On all plots the building height H is defined with a red dotted line. On plots **(a)**, **(c)**, and **(d)** error bars of one standard deviation are displayed in grey representing the uncertainty in the region of the incoming flow that was averaged in the streamwise direction

4 Results

4.1 Centre-Plane Measurements

4.1.1 Mean Velocity Fields

Figure 6 shows PIV mean field characteristics from the planar PIV dataset along the center-line of the building. Figure 6a shows the mean streamwise velocity $\frac{U}{U_\infty}$, close to the tall building. A decrease in velocity in the vicinity of the building is apparent, with this effect continuing much further downstream than upstream. In this figure, the recirculation region is defined by a contour of $\frac{U}{U_\infty} = 0$. This can be seen in the immediate wake attached to the back of the building. The wake recirculation is mostly contained to within 1 H of the trailing edge of the building and has entirely disappeared by 1.4H.

The velocity deficit created by the building is defined as the difference in the local mean flow velocity compared with that measured in the absence of the building, ie. $U - U_{BL}$, where U_{BL} (boundary-layer) is the U value at that point in the boundary layer without the building present. The extent of the region with significant velocity deficit is defined as the contour of $U = 0.95U_{BL}$. Figure 6b shows the extent of the velocity deficit left by the tall

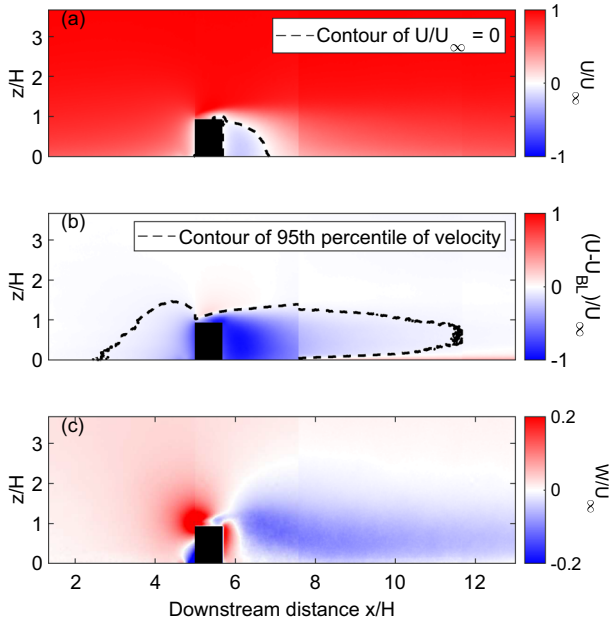


Fig. 6 **a** The extent of the recirculation region in the wake of the tall building, defined as a contour of zero streamwise velocity. Contour is on a plot of normalised streamwise velocity (U/U_∞). **b** The velocity deficit $(U - U_{BL})/U_\infty$ in the wake of the tall building. The extent of this region is defined as a contour of $U = 0.95 * U_{BL}$. **c** The normalised vertical velocity (W/U_∞) in the vicinity of the tall building

building. It extends $7.3H$ downstream of the building, or 221 mm . This is consistent with the findings of Castro and Robins (1977) studies of flow around a wall mounted cube.

Figure 6c is a plot of the mean vertical velocity W/U_∞ . The general pattern shows mostly positive values ahead of the building and mostly negative values in its wake. The flow impinging on the front of the building has a vertical stagnation point on this leading face. Below this point, the mean flow is travelling in the y direction around either side of the building. The large down-wash region in the wake is at a low magnitude but only diminishes in strength slowly and continues into the far-field.

In the case of the CAARC building the recirculation region at ground level extends less than $0.4H$ downstream of the building (Zhao et al. 2022), this length is far lower than the value observed in Fig. 6. This bluff body flow around the isolated building can be likened more easily to the studies of isolated cubes, as done by Castro and Robins (1977), than to studies on the CAARC building (Braun and Awruch 2009; Zhao et al. 2022).

4.1.2 Turbulence Statistics

Figure 7 shows the $\overline{u'w'}$ Reynolds stress component, which is important in the generation of turbulent kinetic energy. This component gives a clear picture of a strong rooftop shear layer, very similar to the one observed by Lim et al. (2022). This $\overline{u'w'}$ shear layer is almost entirely negative, apart from at the leading edge, implying the anti-correlation of the two fluctuating components as expected in a turbulent shear flow. This layer does not significantly spread much further upwards from its starting height above the building, and instead it spreads

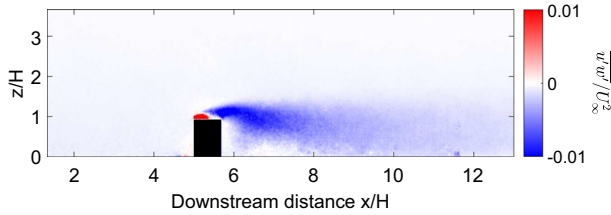


Fig. 7 The $\overline{u'w'}$ Reynolds Stress component around the tall building

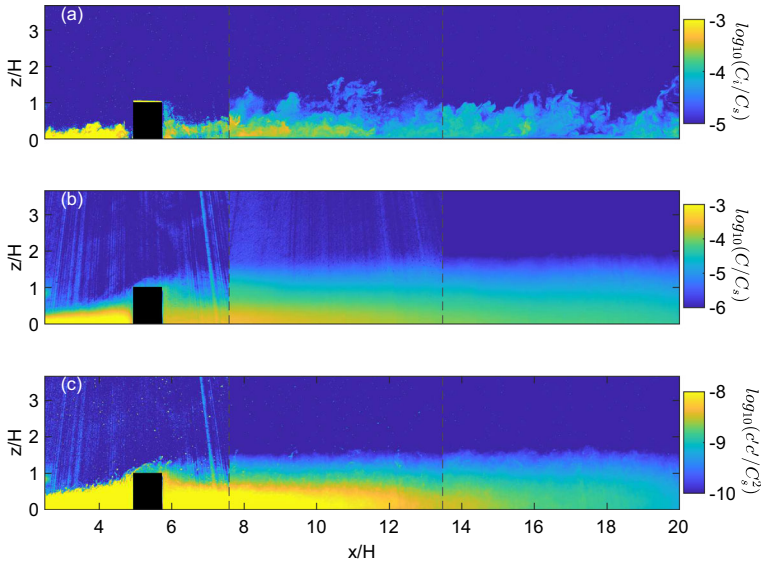


Fig. 8 **a** Three instantaneous slices of species concentration near the tall building on a \log_{10} scale, normalised by the source concentration; the three slices were taken at different times and were later stitched together. **b** The mean species concentration around the tall building on a \log_{10} scale, normalised by the source concentration. **c** The species variance, also normalised by source concentration and shown on a \log_{10} scale. In all three figures dotted lines represent the lines along which different datasets have been stitched together

downwards into the wake behind the building. The recirculation region in the close wake has relatively low Reynolds stress relative to the velocity deficit region.

4.1.3 Species Mean and Variance

An example of the instantaneous concentration field is given in Fig. 8a, which exhibits the high intermittency shown by this plume. This contributes to the low mean concentration values measured far downstream of the building, these are shown in Fig. 8b. The intensity of the dye visible in the instantaneous field is also much higher than the mean values measured. In Fig. 8b, it is also visible that the edge of the plume is driven upwards by the presence of the tall building and continues to expand vertically in the wake of the building.

Figure 8c shows the variance of the concentration in the wake of the tall building. This graph follows the shape of the mean concentration in Fig. 8b. This was also observed in measurements of an unbounded plume in shear flow by Vanderwel and Tavoularis (2014).

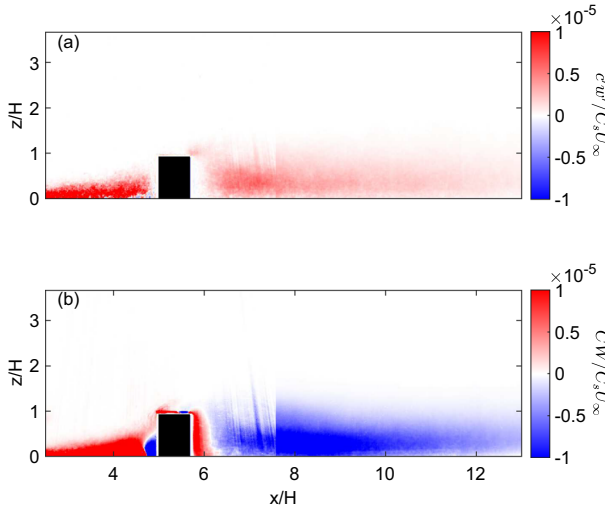


Fig. 9 **a** The vertical turbulent flux field ($\overline{c'w'}/C_s U_\infty$). **b** The vertical advective flux field ($CW/C_s U_\infty$)

The reducing noise in the background of Fig. 8b, c can be attributed to the increasing dye source concentration. Source concentration was increased from 5 mg/l for the measurements around the building to 60 mg/l for downstream. Noise in PLIF measurements often takes the form of laser streaks that are artifacts of the concentration calibration process (Baj et al. 2016).

4.1.4 Scalar Flux Measurements

Figure 9 shows the vertical turbulent and advective fluxes across the centerplane of the flow in the vicinity of the tall building. These fluxes are defined as $\overline{c'w'}$, and CW respectively, in which c is the scalar concentration and w is the vertical velocity component. As scalar concentration values are necessarily positive, the sign of the advective flux field purely corresponds to whether the mean vertical velocity at that point is upwards or downwards. Both turbulent and advective fluxes are extremely low or absent over the top of the tall building, relative to the plume in front of the building. Both scalar fluxes then increase again further in the wake. This is visually exaggerated in Fig. 9a, b, due to the second field of view starting and the signal to noise ratio dramatically improving. The turbulent flux is almost entirely positive, aside from a few points before the tall building, indicating the average effect of turbulence is almost always causing an upwards dispersion of the species, even when the overall flow direction is downwards.

The Fig. 9a, b are displayed on the same colormap and show values of a similar order of magnitude. In almost all locations, the magnitude of the advective flux is slightly greater than the turbulent flux. These results are similar in magnitude and sign to those measured by Lim et al. (2022), the main difference being that the turbulent flux was found to be slightly higher in this isolated building case.

Due to Reynolds analogy, we might expect that locations of high Reynolds stress (ie. turbulent transport of momentum) will also be areas of high vertical turbulent scalar flux (ie. turbulent transport of scalar) (Vanderwel and Tavoularis 2016). However, Fig. 7 shows a high Reynolds stress region above the top of the tall building which does not correlate to a high

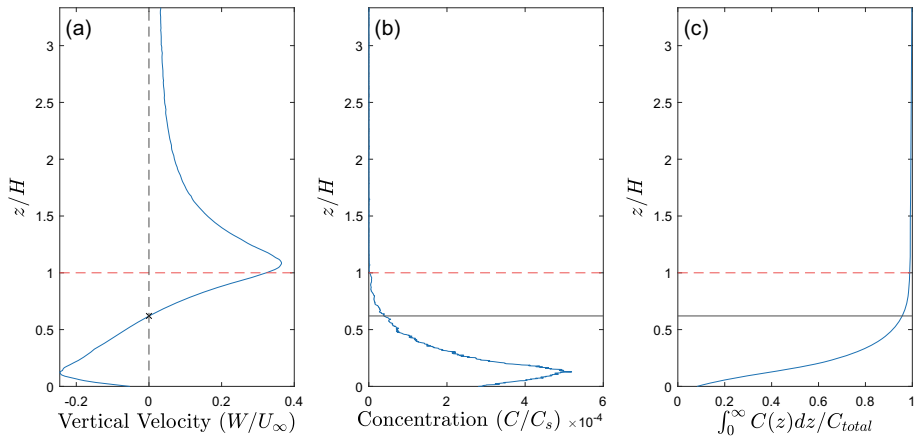


Fig. 10 **a** The mean vertical velocity W (m/s) at the closest PIV measurement to the front of the tall building ($x/H = 4.98$), showing the stagnation point (marked with an X) across this leading face is at $z/H = 0.62$. **b** The concentration profile at the same x location as this PIV measurement, normalised by source concentration. **c** The cumulative total of the concentration profile shown in (b), normalised by the sum of this profile

turbulent scalar flux in the same place in Fig. 9a. This lack of correlation must be due to very little scalar reaching this region. In Fig. 8b it can be seen that the mean concentration above the tall building has dropped multiple orders of magnitude relative to the scalar concentration near the ground, both ahead of and behind the building.

The lack of a region of high turbulent scalar flux above the building in Fig. 9a does not agree with the findings of Lim et al. (2022), which is interesting as both studies use the same building model. Instead Lim et al. (2022) found that while the mean scalar concentration was lower near the ground, it spread significantly above building height. The two differences between these studies are the absence of surrounding buildings in the case presented in this paper, and the distance from the scalar source to the tall building, which is $4H$ in the case presented by Lim et al. (2022) and $5H$ in this case. Lim et al. (2022) shows the scalar plume impinging higher on the tall building than it does in Fig. 8b. This implies that the scalar plume grows faster in the case with surrounding buildings to create low level turbulence despite the lower distance between the building and the plume source. The case presented in this paper only shows the plume reaching the height of the rooftop shear layer when the plume has already passed the building, whereas in the case studied by Lim et al. (2022) the upper edge of it reaches this level before the building.

Figure 10a is a profile of vertical velocity taken immediately ahead of the tall building with the stagnation point and height of the building highlighted. This figure shows that ahead of the tall building vertical velocity is negative up until 62% of the height of the tall building. Integrating the concentration profile shown in Fig. 10b up to this stagnation point and dividing by the total concentration in this profile shows just 6% of the total dye when summed vertically, passes above the stagnation point, with 94% passing below. This process has been illustrated using Fig. 10c. As the advective flux direction always follows that of the mean velocity, and the turbulent flux is generally smaller than the advective flux, the mechanisms transporting dye upwards from this point are minimal. Figure 9 particularly shows that the leading face of the tall building has a very low level of turbulent flux. This means that all scalar impacting below the stagnation point has very little possibility of passing above the building. It needs to already be above this level by the time it reaches the building.

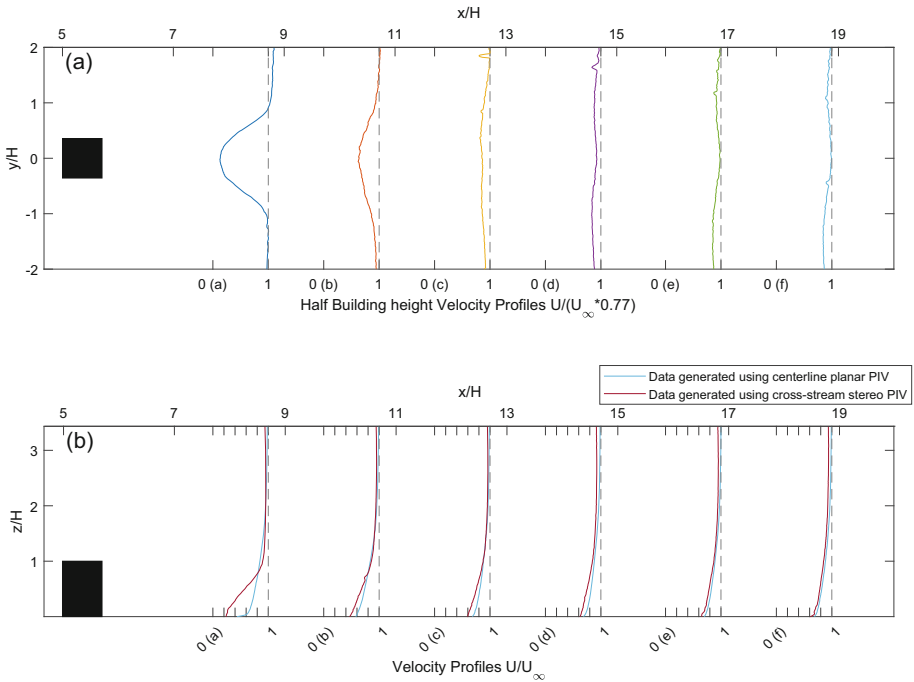


Fig. 11 **a** Cross-stream slices of mean streamwise velocity normalised by the local freestream velocity, this being $0.77 * U_\infty$, as calculated using data shown in Fig. 5a. **b** A comparison of the stereo and planar PIV results at each downstream distance in which stereo data was acquired. Data from planar PIV is shown in light blue, data from stereo PIV is shown in dark red

This lack of transport to the shear layer can possibly explain the lack of presence of any influence from the shear layer in Fig. 9a.

4.2 Cross-Stream Measurements

4.2.1 Mean Velocity

Figure 11a shows the variation in streamwise (U) velocity across the span as measured with the cross-stream stereo PIV. The velocity profiles were extracted at $z/H = 0.5$. These profiles show the velocity deficit in the wake of the tall building diminishing with both downstream and cross-stream distance, and agree with Fig. 6. There is a small asymmetry visible in Fig. 11a and this could be caused by either a small laser sheet misalignment or a small building misalignment with the flow. We can define the distance behind the building as $x - x_B$. This figure shows that beyond $x - x_B = 8H$ ($x = 13.71H$ from source) the flow cross section does not continue to change in a noticeable way.

Figure 11b compares vertical profiles of the streamwise velocity at the same points from both the streamwise 2D PIV and the Stereo-PIV measurements. The measurements agree well with the exception of those obtained at $2H$ downstream of the tall building ($x - x_B = 2H$ or $x = 7.71H$). At this distance, the stereo data shows the most significant change in boundary layer shape from an undisturbed boundary layer. The location is not surprising as this is in

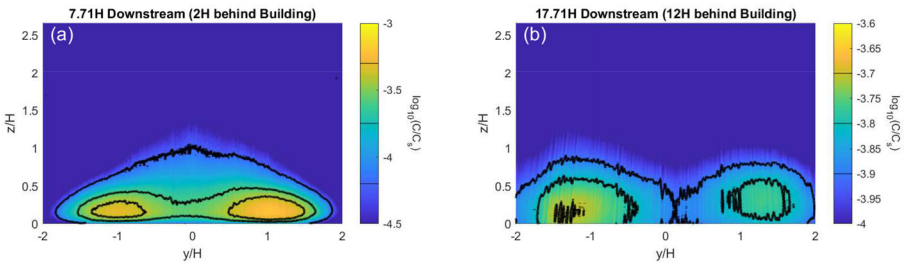


Fig. 12 Species concentration downstream of the tall building on a \log_{10} scale, normalised by source concentration. The values of contour lines are displayed on the colour bars of each figure. Downstream distances shown in (a) and (b) are equal to $x - x_B = 2H$ and $x - x_B = 12H$. Only these two slices were shown for the sake of clarity, the other four are positioned in-between these two and do not reveal anything different to the relationship visible in these two. The two figures are not shown on the same colour map due to the intensity in scalar measured varying significantly between the two planes

a region which is extremely strongly impacted by the velocity deficit. This discrepancy is mostly below $z/H = 0.5$, at the $x - x_B = 2H$ measurement, and it is therefore possible that at this height the laser sheet is introducing uncertainty through reflections off the nearby tall building. This uncertainty being greater is due to the Stereo-PIV experimental setup having the cameras aligned with the out of plane tall building, as shown in Fig. 3. Aside from this measurement the two data sets agree well about the diminishing of the velocity deficit.

4.2.2 Cross-Stream Concentration Measurements

The cross-stream PLIF measurements shown in Fig. 12 show cross-sections of the mean dye concentration at $x - x_B = 2H$ and $x - x_B = 12H$ as the dye plume propagates downstream from the tall building. This figure reveals that the shape of the dye plume has a double peak shape in the wake of the building. The strongest concentration of dye is detected near the ground, but offset to either side of the building. This effect is then less pronounced downstream at $x - x_B = 12H$, however it is still visible. This implies very limited spanwise motion of the species in the far wake. This limited spanwise motion agrees with the measurements of Fuka et al. (2018) when the scalar release is aligned with the front of a tall building.

Figure 12 shows that the highest areas of species concentration are outside the center plane of the flow, once the plume has propagated downstream of the tall building. Most of the species remains trapped close to the floor on either side of the building and then begins to disperse more evenly much further downstream. Comparing this with the understood mechanisms of bluff body aerodynamics (Castro and Robins 1977), it seems that the species is trapped in the horseshoe vortex formed from the base of the bluff body. This horseshoe vortex and bluff body flow structures have been depicted in Fig. 1. The dual-peak plume shape visible in Fig. 12 has not decayed fully as far as $x - x_B = 12H$ downstream of the tall building, implying that an assumption of Gaussian scalar distribution is not accurate until at least beyond this point. Despite the dual plume shape still being visible, it is less distinct at $x - x_B = 12H$. It is presumed that far enough away from the tall building the plume would fully recombine for Gaussian plume theory to be valid.

4.2.3 Turbulent and Advective Structures

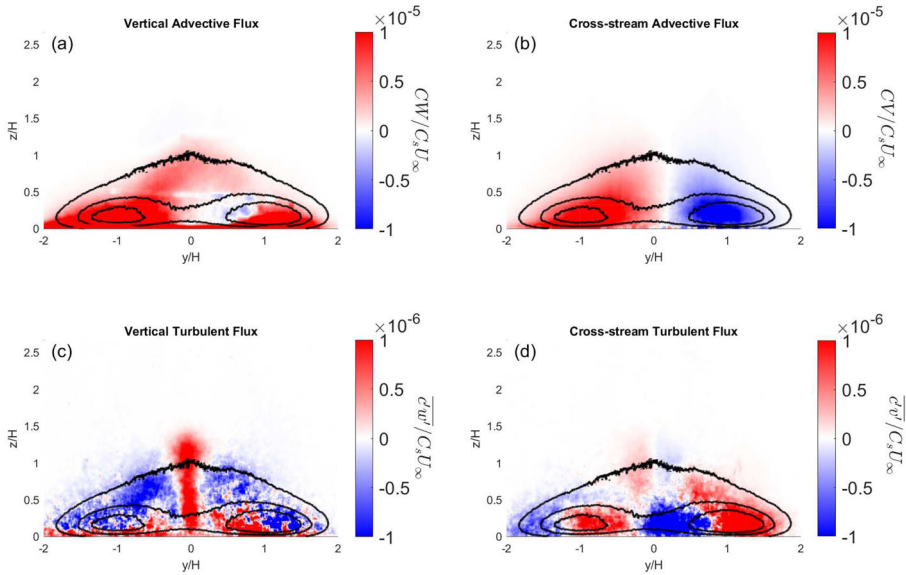


Fig. 13 **a** The Vertical Adjective flux field ($CW/C_s U_\infty$). **b** The Horizontal Adjective flux field ($CV/C_s U_\infty$). **c** The Vertical Turbulent flux field ($\overline{c'w'}/C_s U_\infty$). **d** The Horizontal Turbulent flux field ($\overline{c'v'}/C_s U_\infty$). All plots are taken from $x - x_B = 2H$ downstream of the tall building, or $x = 7.71$ downstream of the dye source. All have contours of mean concentration superimposed for clarity, the values of these contours are visible in Fig. 12a

The vertical advective flux field shown in Fig. 13a shows an upwards motion of the dye throughout most of this slice of the wake of the tall building. This is only present in this slice at $x - x_B = 2H$ and further downstream of the tall building, this flux becomes consistently negative on the center-line. This slice does not agree with the data displayed in Fig. 9b but all other advective fields do agree. The positive vertical advective regions offset from the center in Fig. 13d show a high magnitude and appear to be significant to the development of the plume shape. Figure 13b reveals an overall converging motion of the plume towards the center-line. The region with strong advective flux stays relatively close to the tunnel floor and with the greatest height at which advective flux is measured being on the center-line. However this region barely rises above the building height.

The vertical turbulent flux shown in Fig. 13c agrees with Fig. 9a. However it also reveals that this positive turbulent flux in the wake of the building is localised to the center-line of the flow and not a generally applicable rule to the whole wake. In fact, it is shown that for this wake, the opposite is true and turbulent flux is negative in most places. The center-line vertical transport does not just agree in sign with the planar results, it also agrees accurately in magnitude, which is gratifying given the difficulties in calculating turbulent fluxes from stereo PIV data. Fuka et al. (2018) observed a consistently positive vertical turbulent flux, which is in contrast to the changing signs revealed in Fig. 13b.

The horizontal turbulent fluxes given in Fig. 13d reveal structures alternating in sign that align closely with the overlaid isocontours of mean concentration. These structures show turbulent horizontal fluxes with signs pointing away from the two points of highest mean concentration. These structures do not extend above $0.5H$.

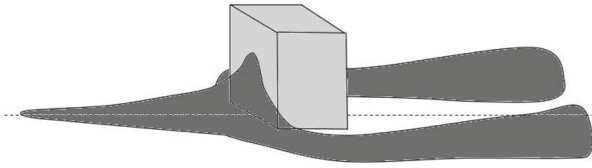


Fig. 14 A diagram of the regions of highest dye concentration, based on the data from both experimental setups. This is intended as a qualitative figure to show the observed effect that the plume is impinging below the building stagnation, and then being trapped in the horseshoe vortex

4.3 Discussion

The hypothesised 3D shape of the highest concentration area of the dye plume is shown in Fig. 14. The downward velocity measured in Fig. 6 represents the extent to which the high concentration area of the species plume extends vertically on the front face of the tall building. It is visible in Fig. 9a, b that both the advective and turbulent vertical scalar fluxes are very low above the tall building, despite the high Reynolds stress being measured in Fig. 7. The low species concentration in the immediate wake is supported by the measurements of Fuka et al. (2018) who observed little cross-stream scalar transport between the horseshoe vortex and the recirculation region of a tall building.

It is presumed that the centerline region is that which is affected by the rooftop shear layer and detached flow at the top of the back of the building. This is based on an extrapolation of the established bluff body flow structures depicted in Fig. 1. However in this experimental case, this region has had a less significant influence on dispersive behavior than in some previous studies (Lim et al. 2022). The diagram given in Fig. 14 essentially reflects a transition from a ground-source plume to the leading edge horseshoe vortex shape trailing behind a bluff body. This diagram differs heavily to the diagram showing all flow structures (Fig. 1) as only the horseshoe vortex was proven to be relevant to dispersion in this particular case. The scalar species becoming trapped in the horseshoe vortex was also measured by Fuka et al. (2018); however, in that case the scalar was released directly into the front of the horseshoe vortex. With how low lying the scalar plume was shown to be in Fig. 8b, it is not surprising that this paper measured a similar pattern of low vertical transport to Fuka et al. (2018).

We can speculate how concentration transport would vary for buildings of different aspect ratios by considering the roles of the horseshoe vortex and the stagnation point. Figure 14 is based on the measurements around a square-cylinder with aspect ratio 1.4 that were done in this study. In the case of a higher aspect ratio building such as the CAARC building, we would expect that less of the scalar will be trapped in the horseshoe vortex due to it being a relatively smaller flow structure. Instead the lateral separation zone (see Fig. 1) would become larger and transport more of the scalar. In the case of a lower aspect ratio structure like a cube, the horseshoe vortex would become stronger again and would be expected to trap an even higher proportion of the dye.

For both speculated examples above the assumption is made that the scalar plume impinges at a similar height relative to the stagnation point. This is because if the plume impinges above the stagnation point then much more of the scalar will enter the recirculation region or wake vortex instead of the horseshoe vortex. The impingement height of the scalar would depend on the position and elevation of the source and how much it has spread before reaching the building. We have also learned that the surrounding geometry also influences the distribution of the concentration reaching the building.

5 Conclusions

The flow structures around a single tall building have been examined using the PIV and PLIF techniques in both streamwise and cross-stream slices. Data has been analysed and compared with existing literature as validation. Vertical scalar fluxes were calculated on the centre plane to compare the components of vertical scalar dispersion. It was found that along the centerplane of the wake, the advective flux stayed negative into the far field, whereas the turbulent flux was smaller but positive, shown in Figs. 9 and 13.

3D analysis of the scalar plume around this building showed a distinct dual peak shape, with a trough along the centerplane of the flow, visible in Fig. 12. This shape was still measurable at the furthest cross stream measurements, 12 H downstream of the tall building.

Comparison with scalar flux measurements by Lim et al. (2022) show that while rooftop shear layer turbulent flux dominated dispersion in that case, it contributed close to nothing in the case studied in this paper. This is hypothesised to be because, without the surrounding buildings creating near wall turbulence, the scalar was not transported into the rooftop shear layer. We showed that overwhelmingly the turbulent flux has an upwards direction. Therefore it can be implied that the lower level of turbulent flux before the building contributes towards the lower plume height when it reaches building. This low plume height then causes the majority of the scalar to become trapped in the horseshoe vortex forming around the base of the tall building.

In summary, the centre plane alone was not sufficient to explain the plume's interactions with flow structures in the wake of the tall building. It is important when studying these structures experimentally to also measure at an offset from the center-plane. Similarly advective fluxes are insufficient to fully explain the plume dispersion. We showed (Fig. 9) that turbulent fluxes are of the same order of magnitude as advective fluxes, and that (Fig. 13) the turbulent fluxes switch direction in more localised patterns than the advective fluxes do. If turbulent fluxes are being modelled in computational simulation then it is important that these inhomogenities are captured accurately.

Acknowledgements We gratefully acknowledge funding from Christina Vanderwel's UKRI Future Leaders Fellowship (MR/S015566/1).

Data availability Data is made available in the University of Southampton data repository at <https://doi.org/10.5258/SOTON/D3158>.

Open Access This article is licensed under a Creative Commons Attribution 4.0 International License, which permits use, sharing, adaptation, distribution and reproduction in any medium or format, as long as you give appropriate credit to the original author(s) and the source, provide a link to the Creative Commons licence, and indicate if changes were made. The images or other third party material in this article are included in the article's Creative Commons licence, unless indicated otherwise in a credit line to the material. If material is not included in the article's Creative Commons licence and your intended use is not permitted by statutory regulation or exceeds the permitted use, you will need to obtain permission directly from the copyright holder. To view a copy of this licence, visit <http://creativecommons.org/licenses/by/4.0/>.

References

- Arya SP et al (1999) Air pollution meteorology and dispersion, vol 310. Oxford University Press, New York
- Baj P, Bruce PJ, Buxton OR (2016) On a PLIF quantification methodology in a nonlinear dye response regime. *Exp Fluids* 57(6):1–19. <https://doi.org/10.1007/s00348-016-2190-0>
- Bermous I, Steinle P (2015) Efficient performance of the Met Office Unified Model v8.2 on Intel Xeon partially used nodes. *Geosci Model Dev* 8:769–779. <https://doi.org/10.5194/gmd-8-769-2015>

- Braun AL, Awruch AM (2009) Aerodynamic and aeroelastic analyses on the CAARC standard tall building model using numerical simulation. *Comput Struct* 87:564–581. <https://doi.org/10.1016/j.compstruc.2009.02.002>
- Castro IP, Robins AG (1977) The flow around a surface-mounted cube in uniform and turbulent streams. *J Fluid Mech* 79:307–335. <https://doi.org/10.1017/S0022112077000172>
- City of London (2022) City of London, Micro climate Guidelines kernel description. <https://www.cityoflondon.gov.uk/services/planning/microclimate-guidelines>
- Dziubanek G, Spychała A, Marchwińska-Wyrwał E, Rusin M, Hajok I, Ćwieląg-Drabek M, Piekut A (2017) Long-term exposure to urban air pollution and the relationship with life expectancy in cohort of 3.5 million people in Silesia. *Sci Total Environ* 580:1–8. <https://doi.org/10.1016/j.scitotenv.2016.11.217>
- Elshaer A, Aboshosha H, Bitsuamlak G, Damatty AE, Dagnew A (2016) Les evaluation of wind-induced responses for an isolated and a surrounded tall building. *Eng Struct* 115:179–195. <https://doi.org/10.1016/j.engstruct.2016.02.026>
- Fackrell JE, Robins AG (1982) Concentration fluctuations and fluxes in plumes from point sources in a turbulent boundary layer. *J Fluid Mech* 117:1–26. <https://doi.org/10.1017/S0022112082001499>
- Fuka V, Xie ZT, Castro IP, Hayden P, Carpentieri M, Robins AG (2018) Scalar fluxes near a tall building in an aligned array of rectangular buildings. *Boundary-Layer Meteorol* 167(1):53–76. <https://doi.org/10.1007/s10546-017-0308-4>
- Hearst RJ, Gomit G, Ganapathisubramani B (2016) Effect of turbulence on the wake of a wall-mounted cube. *J Fluid Mech* 804:513–530. <https://doi.org/10.1017/jfm.2016.565>
- Heist DK, Brixey LA, Richmond-Bryant J, Bowker GE, Perry SG, Wiener RW (2009) The effect of a tall tower on flow and dispersion through a model urban neighborhood: part 1. Flow characteristics. *J Environ Monit* 11:2163–2170. <https://doi.org/10.1039/b907135k>
- Hu X, Morgans AS (2022) Attenuation of the unsteady loading on a high-rise building using feedback control. *J Fluid Mech*. <https://doi.org/10.1017/jfm.2022.467>
- Lim HC, Castro IP, Hoxey RP (2007) Bluff bodies in deep turbulent boundary layers: Reynolds-number issues. *J Fluid Mech* 571:97–118. <https://doi.org/10.1017/S0022112006003223>
- Lim HD, Vanderwel C (2023) Turbulent dispersion of a passive scalar in a smooth-wall turbulent boundary layer. *J Fluid Mech*. <https://doi.org/10.1017/jfm.2023.562>
- Lim HD, Hertwig D, Grylls T, Gough H, Reeuwijk MV, Grimmond S, Vanderwel C (2022) Pollutant dispersion by tall buildings: laboratory experiments and large-eddy simulation. *Exp Fluids*. <https://doi.org/10.1007/s00348-022-03439-0>
- Martinuzzi R, Tropea C (1993) The flow around surface-mounted, prismatic obstacles placed in a fully developed channel flow. *J Fluids Eng* 10(1115/1):2910118
- Met Office (2022) The Cray XC40 supercomputing system kernel description. <https://www.metoffice.gov.uk/about-us/what/technology/supercomputer>
- Plate EJ (1999) Methods of investigating urban wind fields—physical models. *Atmos Environ* 33:3981–3989. [https://doi.org/10.1016/S1352-2310\(99\)00140-5](https://doi.org/10.1016/S1352-2310(99)00140-5)
- Pope SB (2001) *Turbulent flows*, vol 12. Cambridge University Press
- Talluru KM, Philip J, Chauhan KA (2018) Local transport of passive scalar released from a point source in a turbulent boundary layer. *J Fluid Mech* 846:292–317. <https://doi.org/10.1017/jfm.2018.280>
- Tomas JM, Eisma HE, Pourquie MJ, Elsinga GE, Jonker HJ, Westerweel J (2017) Pollutant dispersion in boundary layers exposed to rural-to-urban transitions: varying the spanwise length scale of the roughness. *Boundary-Layer Meteorol* 163(2):225–251. <https://doi.org/10.1007/s10546-016-0226-x>
- United Nations Department of Economic and Social Affairs (2018) 68% of the world population projected to live in urban areas by 2050, says UN kernel description. <https://www.un.org/development/desa/en/news/population/2018-revision-of-world-urbanization-prospects.html>
- Vanderwel C, Tavoularis S (2014) Measurements of turbulent diffusion in uniformly sheared flow. *J Fluid Mech* 754:488–514. <https://doi.org/10.1017/jfm.2014.406>
- Vanderwel C, Tavoularis S (2016) Scalar dispersion by coherent structures in uniformly sheared flow generated in a water tunnel. *J Turbul* 17(7):633–650. <https://doi.org/10.1080/14685248.2016.1155713>
- Williams M, Barrowcliffe R (2011) Review of air quality modelling in defra a report by the air quality modelling review steering group
- Xie ZT, Coceal O, Castro IP (2008) Large-Eddy simulation of flows over random urban-like obstacles. *Boundary-Layer Meteorol* 129(1):1–23. <https://doi.org/10.1007/s10546-008-9290-1>
- Zhao R, Feng Z, Dan D, Wu Y, Li X (2022) Numerical simulation of CAARC standard high-rise building model based on MRT-LBM large eddy simulation. *Shock Vib*. <https://doi.org/10.1155/2022/1907356>